

# Nonlinear instability in flagellar dynamics: a novel modulation mechanism in sperm migration?

H. Gadêlha<sup>1,2,3,\*</sup>, E. A. Gaffney<sup>1,2</sup>, D. J. Smith<sup>2,4,5</sup>  
and J. C. Kirkman-Brown<sup>2,5</sup>

<sup>1</sup>*Centre for Mathematical Biology, Mathematical Institute, University of Oxford,  
24–29 St Giles', Oxford OX1 3LB, UK*

<sup>2</sup>*Centre for Human Reproductive Science, Birmingham Women's NHS Foundation Trust,  
Edgbaston, Birmingham, UK*

<sup>3</sup>*The Capes Foundation, Ministry of Education of Brazil, Cx. Postal 365,  
Brasília 70359-970, Brazil*

<sup>4</sup>*School of Mathematics, and* <sup>5</sup>*School of Clinical and Experimental Medicine,  
University of Birmingham, Edgbaston, Birmingham B15 2TT, UK*

Throughout biology, cells and organisms use flagella and cilia to propel fluid and achieve motility. The beating of these organelles, and the corresponding ability to sense, respond to and modulate this beat is central to many processes in health and disease. While the mechanics of flagellum–fluid interaction has been the subject of extensive mathematical studies, these models have been restricted to being geometrically linear or weakly nonlinear, despite the high curvatures observed physiologically. We study the effect of geometrical nonlinearity, focusing on the spermatozoon flagellum. For a wide range of physiologically relevant parameters, the nonlinear model predicts that flagellar compression by the internal forces initiates an effective buckling behaviour, leading to a symmetry-breaking bifurcation that causes profound and complicated changes in the waveform and swimming trajectory, as well as the breakdown of the linear theory. The emergent waveform also induces curved swimming in an otherwise symmetric system, with the swimming trajectory being sensitive to head shape—no signalling or asymmetric forces are required. We conclude that nonlinear models are essential in understanding the flagellar waveform in migratory human sperm; these models will also be invaluable in understanding motile flagella and cilia in other systems.

**Keywords:** sperm motility; buckling instability; nonlinear flagellar dynamics; symmetry breaking; asymmetric waveforms; internally driven filaments

## 1. INTRODUCTION

Spermatozoan motility is critical for fertilization and relies on the whip-like beating of a flagellum. This waveform arises through an intricate balance of internally generated shear, flagellar elastic resistance and hydrodynamic viscous drag. Despite complex beat patterns, aspects of the overall swimming trajectories are simply related to properties of flagellar bending. In particular, averaged over a beat cycle, symmetrical flagellar waveforms propel free swimming cells in relatively straight paths (Gray & Hancock 1955; Katz *et al.* 1989; Smith *et al.* 2009*a,b*), while bending asymmetry drives the cell in curved trajectories, as illustrated in figure 1*b*. Furthermore, when the sperm head is pinned to a surface, beat asymmetry induces cell rotation about the point of attachment (Goldstein 1977). Asymmetric

bending has also been observed to be important in the chemotactic response of sperm (Miller & Brokaw 1970; Wolgemuth *et al.* 2000) and during hyperactivation (Katz *et al.* 1989; Kinukawa *et al.* 2003), a motility change that is thought to be required for successful fertilization. However, despite the vital role of symmetry-breaking phenomena for the flagellar waveform, and consequently for sperm transport, the mechanism by which asymmetric beating is generated is yet to be fully understood.

Domain boundaries can also induce asymmetric dynamics (Katz *et al.* 1989). When sufficiently close to a solid boundary, typically at a distance of less than the sperm body length, numerous swimming behaviours have been observed. Rodent sperm with hook-like heads often swim with a planar flagellar waveform and a trajectory curvature of fixed chirality relative to the sperm head. This is considered to arise from the influence of head geometry on stable surface swimming (Woolley 2003). Similarly, for sperm with more symmetrical heads, non-planar beating can

\*Author for correspondence (gadelha@maths.ox.ac.uk).

Electronic supplementary material is available at <http://dx.doi.org/10.1098/rsif.2010.0136> or via <http://rsif.royalsocietypublishing.org>.

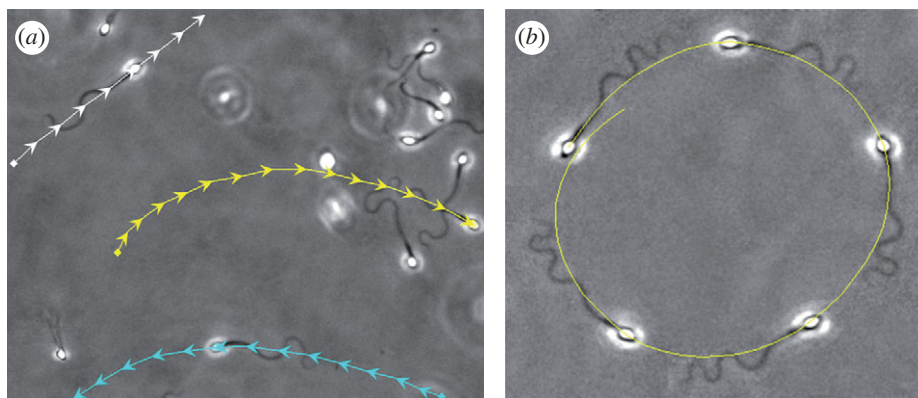


Figure 1. Imaging frames for non-rolling human sperm cells migrating within a viscous medium, containing 2% methyl-cellulose, in a capillary chamber of  $400\ \mu\text{m}$  depth, captured at the same focal plane: (a) swimming trajectories (arrows) for three cells, indicated in white, yellow and cyan and plotted at the same time interval,  $0.4\ \text{s}$  (electronic supplementary material, movie S1). (b) A circularly swimming cell further along the capillary chamber; the imaging sequence is superimposed at equal time intervals of  $2\ \text{s}$ , with the swimming trajectory given by the yellow curve. For further details about the microscopy materials and methods, see electronic supplementary material.

occur with cell rolling during surface swimming, resulting in circular swimming trajectories in the direction of cell rolling, which is always the same within a species (Woolley 2003).

Surfaces do not always appear to dictate the symmetry breaking of sperm cells. This is illustrated in figure 1a, for non-rolling human sperm that have migrated significant distances within a deep chamber ( $400\ \mu\text{m}$ ) filled with a physiological high-viscosity medium. Here, clockwise (yellow) and counterclockwise (cyan) surface swimmers can be observed together with an approximately straight swimming path (white). In this case, no obvious morphological feature dictates the chirality of path curvature. In figure 1b, the manifest asymmetrical bending associated with circular swimming is also illustrated.

These observations readily establish that symmetry breaking and curved trajectories can occur without cell rolling or asymmetric cell morphology and need not be driven by dominant boundary influences. In such cases, it is not clear that an internal asymmetry of the flagellum is dynamically important and driving symmetry breaking, whether it be due to an asymmetric force generation by the dynein molecular motors, as indicated in hyperactivation arising from elevated intracellular calcium (Suarez & Ho 2003), or the subtle heterogeneities of flagellar structure (Fawcett 1975). This is especially the case for species such as humans that can also exhibit highly symmetric waveforms. Thus, our aim is to explore whether physical principles support the null hypothesis that asymmetric waveforms can be generated within flagella with no intrinsic asymmetry and without asymmetric internal forces via a dynamical instability, as observed with passive filament bending in viscous shear flows (Becker & Shelley 2001). In the following study, we therefore summarize relevant features of flagellar mechanics, construct a simple elastohydrodynamical model exploring flagella waveform symmetry breaking for sperm motility within viscous, Newtonian, fluids and, finally, place the findings in the context of sperm motility through numerical simulations and a parameter study.

## 2. FLAGELLAR MECHANICS

The elastohydrodynamic formulation, which couples the structural mechanics of the flagellum with the surrounding fluid, has been extensively studied (Machin 1958; Brokaw 1971, 1975; Hines & Blum 1978; Lindemann & Kanous 1995; Camalet *et al.* 1999; Camalet & Jülicher 2000; Riedel-Kruse *et al.* 2007; Fu *et al.* 2008; Hilfinger & Jülicher 2008; Hilfinger *et al.* 2009), both experimentally and theoretically. In the founding study, Machin (1958) proposed that an internal forcing mechanism was required to maintain the flagellar bending observed in spermatozoa experiments. This hypothesis was later established with the discovery of the axoneme internal structure, revealing that sliding microtubules drive active flagellar bending (Satir 1965). Although Brokaw first considered this microtubule sliding mechanism in modelling flagellar locomotion (Brokaw 1971, 1975), the nonlinear flagellar elastohydrodynamic equations were only derived several years later by Hines & Blum (1978). Later, analogous, models have also been proposed in the literature, exploring both linear (Camalet *et al.* 1999; Camalet & Jülicher 2000; Riedel-Kruse *et al.* 2007; Fu *et al.* 2008) and more recently weakly nonlinear dynamics (Hilfinger *et al.* 2009).

Despite such progress in modelling the internally driven flagellum, the influence of dynamical nonlinear instabilities on the emergent flagellar beat pattern and the consequences for cell swimming have been largely neglected. Nonetheless, nonlinear instabilities are well established for the biophysical dynamics of slender-body systems, including gliding motility assays of cytoskeletal filaments with flow defects (Bourdieu *et al.* 1995), torque-induced writhing of a rotating elastica (Wolgemuth *et al.* 2000) and the behaviour of passive filaments within shear flows (Becker & Shelley 2001). The latter in particular highlights that instabilities can emerge from filament compression, with a sharp transition to buckling followed by complicated shape perturbations. Recent studies of flagellar waveform mechanics have initiated explorations of

internally generated shear between the microtubules via a linear formulation (Camalet *et al.* 1999; Camalet & J licher 2000; Riedel-Kruse *et al.* 2007; Fu *et al.* 2008), as well as considering the lowest order nonlinear effects on the self-organized bending waves (Hilfinger *et al.* 2009). These investigations highlight that the emergent axonemal beat patterns are a good approximation to the weakly nonlinear problem (Hilfinger *et al.* 2009). However, except for a brief, perturbative, study on the role of tension owing to an external force (Camalet & J licher 2000), the possibility that nonlinear tension dynamics can induce dynamical symmetry breaking has been widely neglected in active flagellar mechanics. Furthermore, this entails that the range of validity of the linear model is not completely explored.

Thus, in contrast to the vast majority of works on the internally driven filament, we investigate whether flagellar tension can induce symmetry breaking via a buckling mechanism and how it may influence flagellar beating and sperm swimming trajectories. This requires considering geometrical nonlinearities in flagellar models coupling internal shear generation via microtubule sliding, the flagellum elastic response and viscous drag. In addition, we also explore the agreement between the geometric nonlinear theory and the linear approximation. This will allow us to delimit the region of validity of linear theory in parameter space, further bridging the gap between linear and nonlinear regimes. In turn, such studies will be important for the formulation of well-founded models for forced elastohydrodynamic problems in the future.

### 2.1. Elastohydrodynamic formulation

We consider an internally driven sperm flagellum with a planar waveform, immersed within a viscous fluid. Inertial effects are negligible, because of the very low Reynolds number of sperm swimming, while the hydrodynamic interactions are simplified using resistive-force theory (RFT; Gray & Hancock 1955). This local drag model is the leading order term of the equations of slender-body hydrodynamics (Johnson 1980), and it is simply specified by a local linear relation between the velocity of the flagellum centreline and the force (per unit length) exerted on the fluid, through the anisotropic drag coefficients. Although RFT is only valid for very slender filaments, it is widely used for general elastohydrodynamic problems, including relaxational and forced dynamics of stiff polymers (Machin 1958; Bourdieu *et al.* 1995; Goldstein & Langer 1995; Goldstein *et al.* 1998; Wiggins *et al.* 1998; Wolgemuth *et al.* 2000; Becker & Shelley 2001; Yu *et al.* 2006), as well as flagellar dynamics (Machin 1958; Brokaw 1971; Hines & Blum 1978; Johnson & Brokaw 1979; Lindemann & Kanous 1995; Camalet *et al.* 1999; Camalet & J licher 2000; Riedel-Kruse *et al.* 2007; Fu *et al.* 2008; Hilfinger & J licher 2008; Hilfinger *et al.* 2009), among others. Theoretical predictions using RFT have previously shown a remarkably good agreement with experimental measurements for actuated filaments (Wiggins *et al.* 1998; Yu *et al.* 2006) and the buckling instability exhibited by a single passive filament within a

shear flow (Becker & Shelley 2001; Tornberg & Shelley 2004). In addition, microscopy imaging (Riedel-Kruse *et al.* 2007) has also confirmed that RFT is surprisingly accurate when applied to bull sperm flagellar dynamics, while numerical simulations accounting for non-local hydrodynamic effects support the use of RFT for microswimmers with relatively small cell bodies, including human sperm (Johnson & Brokaw 1979).

Sperm flagellar motion is driven by dynein motor proteins, exerting a relative shearing force between outer adjacent filaments, or microtubules, of the flagellar axoneme: this is referred to as the sliding filament model (Brokaw 1971, 1975; Hines & Blum 1978; Camalet *et al.* 1999; Camalet & J licher 2000; Riedel-Kruse *et al.* 2007; Fu *et al.* 2008; Hilfinger & J licher 2008; Hilfinger *et al.* 2009). For planar flagellar waveforms of mammalian sperm, there is a preferred plane of beating imposed by the mammalian flagellar accessory structures (Lindemann *et al.* 1992). In this context, faithful three-dimensional descriptions of the cylindrical arrangement of microtubule doublets in mammalian sperm have been shown to be equivalent to a simpler two-dimensional representation of the sliding forces within the axoneme, as depicted in figure 2 (Hilfinger & J licher 2008; Hilfinger *et al.* 2009). Here, a pair of parallel elastic filaments may slide relative to each other within the beat plane in response to dynein forces. Each sliding filament is assumed to be homogeneous, inextensible and separated by a constant gap spacing  $b$ , which corresponds to the axoneme diameter. At the sperm head junction, we assume for simplicity that no interfilament shear is permitted owing to structural constraints. The axoneme motor proteins induce active shear stresses along the flagellum, which act in opposite directions and force the filaments to locally slide with respect to each other, inducing flagellar bending (figure 2).

### 2.2. Geometrically nonlinear theory: equation of motion

It is convenient to describe the flagellum position, relative to the laboratory frame of reference, by its neutral line  $\mathbf{X}(s, t)$  (figure 2), noting that  $t$  is time and  $s$  denotes the distance along the flagellum with  $0 \leq s \leq L$ , where  $L$  is the filament length. The local flagellum coordinate system is represented as an orthonormal pair with a positive orientation  $(\hat{\mathbf{s}}(s, t), \hat{\mathbf{n}}(s, t))$ , where  $\hat{\mathbf{s}} = \mathbf{X}_s \equiv \partial \mathbf{X} / \partial s$  is the tangent vector and  $\hat{\mathbf{n}}$  is the vector normal to the flagellum centreline (figure 2). The flagellar dynamics is inertialess and simply arises via balancing the viscous drag force per unit length with the internal forces per unit length within the flagellum. Non-dimensionalizing with respect to the length scale  $L$ , time scale  $\omega^{-1}$  and force density  $E/L^3$ , for a given beating frequency  $\omega$  and constant flagellum elastic stiffness  $E$ , the *dimensionless* elastohydrodynamic equation of motion for the flagellum neutral line reads

$$\text{Sp}^4 \mathbf{X}_t = -\mathbf{X}_{ssss} - (\gamma - 1)(\mathbf{X}_s \cdot \mathbf{X}_{ssss})\mathbf{X}_s + (T\mathbf{X}_{ss} + \gamma T_s \mathbf{X}_s) + (f_s \hat{\mathbf{n}} + \gamma f \hat{\mathbf{n}}_s). \quad (2.1)$$

Here, the subscript  $t$  denotes differentiation with respect to time,  $f(s, t)$  is shear force density within the

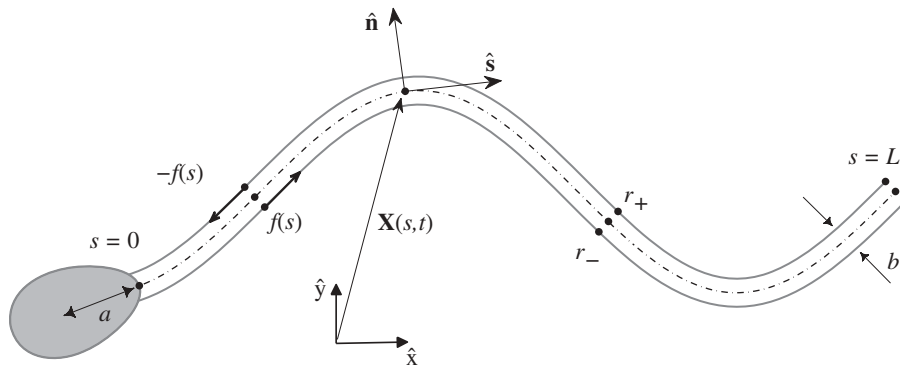


Figure 2. A schematic of the sliding filament mechanism. Relative to a laboratory fixed frame  $\{\hat{x}, \hat{y}\}$ , the vector  $\mathbf{X}(s, t)$  describes the position of the point which is an arclength  $s$  along the flagellum neutral line (dashed curve) at time  $t$ . The internal shear force  $f(s, t)$  is acting tangentially and in opposite directions on each sliding filament  $r \pm(s)$  (solid grey curves) causing the flagellum to bend. The distance between the centre of mass of the sperm head and the flagellum junction is denoted by  $a$  and the flagellar axoneme diameter is  $b$ .

flagellum and  $\gamma = \xi_{\perp} / \xi_{\parallel}$  is the ratio between the perpendicular,  $\xi_{\perp}$ , and parallel,  $\xi_{\parallel}$ , fluid dynamic resistance coefficients. The *sperm-compliance parameter*

$$\text{Sp} = L \left( \frac{\omega \xi_{\perp}}{E} \right)^{1/4} \quad (2.2)$$

is dimensionless and characterizes the relative importance of elastic forces to viscous drag (Wiggins *et al.* 1998). The tensile force  $T(s, t)$  is related to the Lagrange multiplier for inextensibility, and it is implicitly determined by the constraint  $\mathbf{X}_s \cdot \mathbf{X}_s = 1$ . Under appropriate variable transformations, these equations are equivalent to earlier models proposed by Hines & Blum (1978), Gueron & Liron (1993) and Camalet & Jülicher (2000). A detailed derivation is presented in the electronic supplementary material as well as the explicit form of the inextensibility constraint.

Although the sliding filament mechanism has been successful in explaining flagellar bending, there is a limited quantitative understanding of the regulation and nature of the internal shear stress  $f$ , which represents the coupling between the dynein molecular motor activity and the passive cross-linking proteins within the flagellum (Brokaw 2009; Mitchison & Mitchison 2010). There have been several attempts to explain the observed flagellar beat via different shear-control hypotheses dictating the regulation of internal shear  $f$  (Brokaw 1971, 1975, 2009; Hines & Blum 1978; Lindemann & Kanous 1995; Camalet *et al.* 1999; Camalet & Jülicher 2000; Mitchison & Mitchison 2010), although comparison with experiments has only become possible recently (Riedel-Kruse *et al.* 2007). Here, it is beyond the scope of the study to consider detailed assessments of the internal shear regulation and the difficulties associated with dynein control mechanisms. Instead, we use a symmetric model, based on observations of shear *in situ*, to explore the symmetry-breaking event. As detailed in the electronic supplementary material, travelling waves of bending (Smith *et al.* 2009b), and thus internal shear forces, periodically propagate down the flagellum; given that the dominant mode typically dictates the dynamics (Riedel-Kruse *et al.* 2007), we therefore

model the internal shear density as a simple travelling wave

$$f(s, t) = A \cos(ks - t), \quad (2.3)$$

with dimensionless force amplitude  $A$  and wavenumber  $k$ . This particular choice of internal shear will not just isolate the potential for symmetry breaking of a symmetrically driven flagellum, it will also enable us to investigate a wide range of shear distribution  $k$ , bringing to light new nonlinear effects within a general framework.

### 2.3. Boundary conditions

The equations governing the flagellar dynamics are closed by defining the initial cell configuration together with the boundary conditions, in which either the movement of the flagellar endpoints is specified or a balance of forces and torques at each end is imposed. In particular, at the distal boundary,  $s = L$ , the flagellum is free to move and, therefore, the external torques and forces are zero, i.e.

$$\mathbf{M}_{\text{ext}} = \mathbf{F}_{\text{ext}} = 0 \quad \text{at} \quad s = L.$$

At the proximal end of the flagellum,  $s = 0$ , we consider three distinct boundary conditions motivated by laboratory examples:

- *The clamped head.* The sperm head is strongly adhered, with no rotation about its point of attachment, so that both its position and tangent vectors are fixed:  $\mathbf{X}_t|_{s=0} = \mathbf{X}_{st}|_{s=0} = 0$ .
- *The pivoting head.* The sperm head is adhered so that it does not move except for rotation about its attachment, due to the absence of an external moment:  $\mathbf{X}_t|_{s=0} = \mathbf{M}_{\text{ext}}|_{s=0} = 0$ .
- *The swimming sperm.* The cell body experiences a hydrodynamic viscous drag force,  $\mathbf{F}_{\text{head}}$ , and moment,  $\mathbf{M}_{\text{head}}$ , which are balanced by the contact force and torque between the sperm head and the flagellum at their junction. This balance yields the required boundary condition for the flagellum in terms of the motion of the sperm head via a specification of  $\mathbf{X}_t|_{s=0}$  and  $\mathbf{X}_{st}|_{s=0}$ .

The full nonlinear numerical scheme, using methods similar to (Tornberg & Shelley 2004), validation and derivation of the boundary equations are summarized in the electronic supplementary material.

#### 2.4. Parallels with the linear theory

For small deflections, Camalet & J licher (2000) have shown that the equation of motion (equation (2.1)) simplifies to

$$\text{Sp}^4 h_t = -h_{ssss} + f_s, \quad (2.4)$$

where  $x \approx s$  and  $\mathbf{X}(s, t) \approx s\hat{\mathbf{x}} + h(s, t)\hat{\mathbf{y}}$ . The tensile forces only contribute at subleading orders, and hence  $T(s, t) \approx 0$ . In the absence of internal shear, equations (2.1) and (2.4) describe the elastohydrodynamics of a passive filament in a viscous fluid and have already been studied analytically (Machin 1958; Bourdieu *et al.* 1995; Goldstein & Langer 1995; Goldstein *et al.* 1998; Wiggins *et al.* 1998; Wolgemuth *et al.* 2000; Fu *et al.* 2008) and experimentally (Bourdieu *et al.* 1995; Wiggins *et al.* 1998; Yu *et al.* 2006). Despite the relative simplicity of the linearized formulation equation (2.4), there has not been a study of its accuracy compared with the full nonlinear framework equation (2.1) given the variation of parameters such as the shear force wavenumber  $k$ , shear force amplitude  $A$  and the sperm compliance  $\text{Sp}$ . This was circumvented in Fu *et al.* (2008) by choosing the sliding force amplitude  $A$ , for a given  $\text{Sp}$  and  $k$ , so that the maximum deflection of the filament was no larger than 10 per cent of the total filament length  $L$ . More recently, J licher and collaborators (Hilfinger *et al.* 2009) have considered the role of leading nonlinear contributions in a perturbative formulation and demonstrated that the linear theory provided a good estimate, with no evidence of a buckling instability.

### 3. RESULTS

Numerical simulations were carried out assuming a fluid dynamic resistance ratio  $\gamma = 2$ . Once the boundary conditions are specified, there are two further degrees of freedom: the sperm-compliance parameter  $\text{Sp}$  and the wavenumber  $k$ . Given these, the force amplitude  $A$  is fixed by the constraint that the maximum flagellar displacement does not exceed 10 per cent of the flagellar length in the linear theory, that is,  $\max_{s,t}|h| = 0.1$  in equation (2.4), as in Fu *et al.* (2008). The force amplitude  $A$  is plotted for the clamped and pivoting boundary conditions in electronic supplementary material, figure S1, and the parameter regimes considered are consistent with typical physical quantities observed in spermatozoa experiments (Baltz *et al.* 1990; Lindemann *et al.* 2005; Smith *et al.* 2009*b*). As detailed in the electronic supplementary material, estimates for the human sperm-compliance parameter for various media range from  $\text{Sp} = 4$  to  $\text{Sp} = 24$ , which dictates the choice of  $\text{Sp}$  in the illustrative examples below. We also display results for smaller  $\text{Sp}$ , as low as unity, for completeness, when assessing the validity of the linear theory as other flagellates can operate at smaller compliance numbers, as briefly discussed in the electronic supplementary material.

#### 3.1. Clamped head and pivoting head results

We begin our investigation by contrasting the nonlinear flagellar dynamics equation (2.1) with its linear approximation equation (2.4), with illustrations of the symmetry-breaking behaviour, for the clamped and pivoting head boundary conditions. Figure 3*a–l* shows the time evolution of the linear and nonlinear flagellar shapes for both clamped and pivoting boundary conditions, and six different pairs of wavenumber and sperm compliance parameter ( $k$ ,  $\text{Sp}$ ). Figure 3*m–x* additionally illustrates the time evolution of the nonlinear model predictions for the flagellar beat pattern when symmetry breaking occurs for a range of internal shear wavenumbers,  $k$ , and sperm compliance  $\text{Sp} = 19$  for the clamped head plus sperm compliance  $\text{Sp} = 15$  for the pivoting head.

The linear theory provides a good agreement with the full nonlinear problem for cases *a*, *b*, *g*, *h* and *d*, *e*, *j*, *k* in figure 3. In contrast, the linear approximation fails for cases *c*, *i*, *f*, *l* in figure 3 for both the pivoting and clamped boundary conditions, where the nonlinear solutions are characterized by condensed or highly asymmetric waveforms, breaking up-down symmetry in the plane. This is despite the constraint on the maximum flagellum amplitude, as illustrated for  $k = 5\pi$  and  $\text{Sp} = 12$  in figure 3*f*. The symmetry-breaking behaviour within the nonlinear model is further highlighted in figure 3*m–x*. In particular, at large values of the sperm-compliance parameter,  $\text{Sp}$ , corresponding to increasing viscous domination of the dynamics, the symmetry-breaking behaviour is particularly enhanced. For clamped head boundary conditions, the emergent asymmetrical waveforms are relatively constrained as the tangent vector is also pinned at  $s = 0$ , whereas asymmetrical bending causes the flagellum to rotate about the point of attachment for the pivoting head boundary condition. We also observe that all flagellar patterns are eventually periodic in time, once transients have decayed, despite the complexity in the dynamics, though the period is greatly increased once symmetry breaking has occurred.

To delimit the values of the internal shear force wavenumber,  $k$ , and sperm compliance parameter,  $\text{Sp}$ , simulations were performed for  $0 \leq k \leq 10\pi$ ,  $1 \leq \text{Sp} \leq 20$ . A measure of the discrepancy between the linear theory predictions for the flagellar waveform,  $\mathbf{X}_L(s, t)$ , and the nonlinear theory predictions,  $\mathbf{X}_N(s, t)$ , is given by

$$D_{\max} = \max_{s,t} |\mathbf{X}_N(s, t) - \mathbf{X}_L(s, t)|.$$

When  $D_{\max} = 0$ , the agreement is perfect, while if  $D_{\max} \approx 0.1$  or less, the agreement is observed to be qualitatively reasonable. For example in figure 3*e, c*,  $D_{\max} = 0.08$  and  $0.11$ , respectively, whereas in figure 3*i*,  $D_{\max} = 0.47$ .

In figure 4*a, b*,  $D_{\max}$  is plotted as an interpolated function of  $\text{Sp}$  and  $k$ , with the black contour given by  $D_{\max} = 0.1$ . The linear theory is increasingly inaccurate as the sperm compliance parameter,  $\text{Sp}$ , increases even for moderate internal shear force wavenumbers,  $k$ , especially for the pivoting head boundary conditions. In figure 4*c, d*, the linear theory prediction for the global maximum curvature,  $\kappa_{\max}$ , is plotted as the

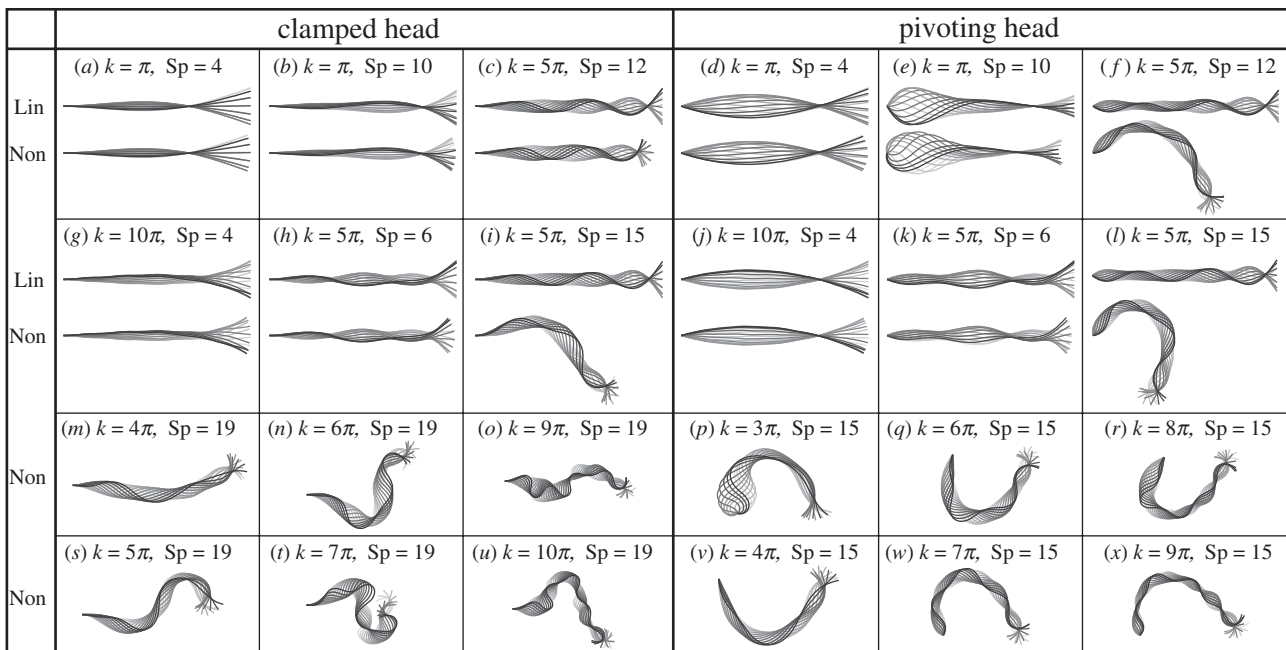


Figure 3. Snapshots of the flagellar evolution for the clamped and pivoting head boundary conditions, plotted at equal time intervals (darker curves for later times). The internal sliding force is given by equation (2.3) for  $\pi \leq k \leq 10\pi$  and  $4 \leq \text{Sp} \leq 19$ , as indicated, and the dimensionless force magnitude  $A$  is chosen to produce a maximum flagellum amplitude of  $0.1L$  in equation (2.4) (electronic supplementary material, figure S1). (a–l) Comparison of the time evolution for the linear (Lin) and nonlinear (Non) theory. Note that the linear theory fails to predict the flagellar shape for cases (c, i, f, l), and that the pivoting boundary condition is more sensitive to the influence of the nonlinear dynamics. (m–x) Typical symmetry-breaking shapes, characterized by an ‘S’ for clamped boundary conditions (Sp = 19) and a ‘C’ for pivoting boundary conditions (Sp = 15). Furthermore, all beating patterns are periodic in time, despite their appearance.

sperm compliance Sp and wavenumber  $k$  are varied, with the contour  $D_{\max} = 0.1$  once more given by a solid black curve. Clearly, there is a strong positive correlation between the maximum curvature obtained from the linear model and the discrepancy measure,  $D_{\max}$ , for both boundary conditions, explicitly highlighting that the linear theory becomes inaccurate as its predictions for flagellar curvature increase. In particular, once the radius of curvature is less than, approximately, 10 per cent of the flagellar length ( $\kappa_{\max} = 10$ ), the linear theory is observed to be unreliable.

One should note that figure 4b,d exhibits a blank region in the upper left corner. The high flagellar compliance, slowly varying internal shear distribution and flagella hinging characterizing this region of parameter space allow a local build-up of high curvature and tension, with sudden changes in the force direction. Discretizing the nonlinear equations produces matrices that are too ill-conditioned for reliable simulation. This region of parameter space will not be considered further.

The symmetry-breaking transient dynamics is illustrated in figure 4e,f, where we, respectively, display the flagellar pattern and absolute tension as the buckling instability progresses for the pivoting head boundary conditions with  $k = 6\pi$  and Sp = 15 (figure 3q). During this instability, a common feature is a large absolute tension concentrated towards the sperm cell–flagellum junction at  $s = 0$ , noting that the tension is zero at the distal flagellum,  $s = L$ . After reaching a critical value of absolute tension, the beating shape instability is followed by a sudden drop in the absolute tension together with an increase in the

period (figure 4f). Also, it is noteworthy that the quantity  $D_{\max}$ , displayed in figure 4a,b, or  $\kappa_{\max}$ , plotted in figure 4c,d, can be used as a bifurcation diagram to identify the parameter regimes where the buckling-type instability occurs, since inaccuracies of the linear theory are always observed to be accompanied by this dynamic symmetry-breaking behaviour.

### 3.2. Swimming sperm

We examine the influence of the flagellar buckling instability on swimming sperm. We have considered the effect of two different head morphologies: a ‘human-like’ sperm head (Smith *et al.* 2009a) with dimensions  $4.5 \times 2.8 \times 1.12 \mu\text{m}$  and a spherical head with diameter  $2.40 \mu\text{m}$  so that it has the same volume. The swimming sperm was found to be less sensitive to the flagellar buckling instability, although once both the sperm compliance, Sp, and the internal shear wavenumber,  $k$ , are large, sperm swimming is observed to be profoundly altered by the symmetry-breaking mechanism. The transition in behaviour is, however, smooth and drives the sperm towards swimming in circular paths of constant radius. Furthermore, a small (large) sperm head viscous drag leads to larger (smaller) circular paths. The sperm trajectories for both human-like (dashed red) and spherical head (dashed blue), when  $k = 10\pi$  and Sp = 20, are illustrated in figure 4g. In addition, the swimming direction in figure 4g changes from clockwise to counterclockwise if  $f \rightarrow -f$  in equation (2.1), illustrating that overall

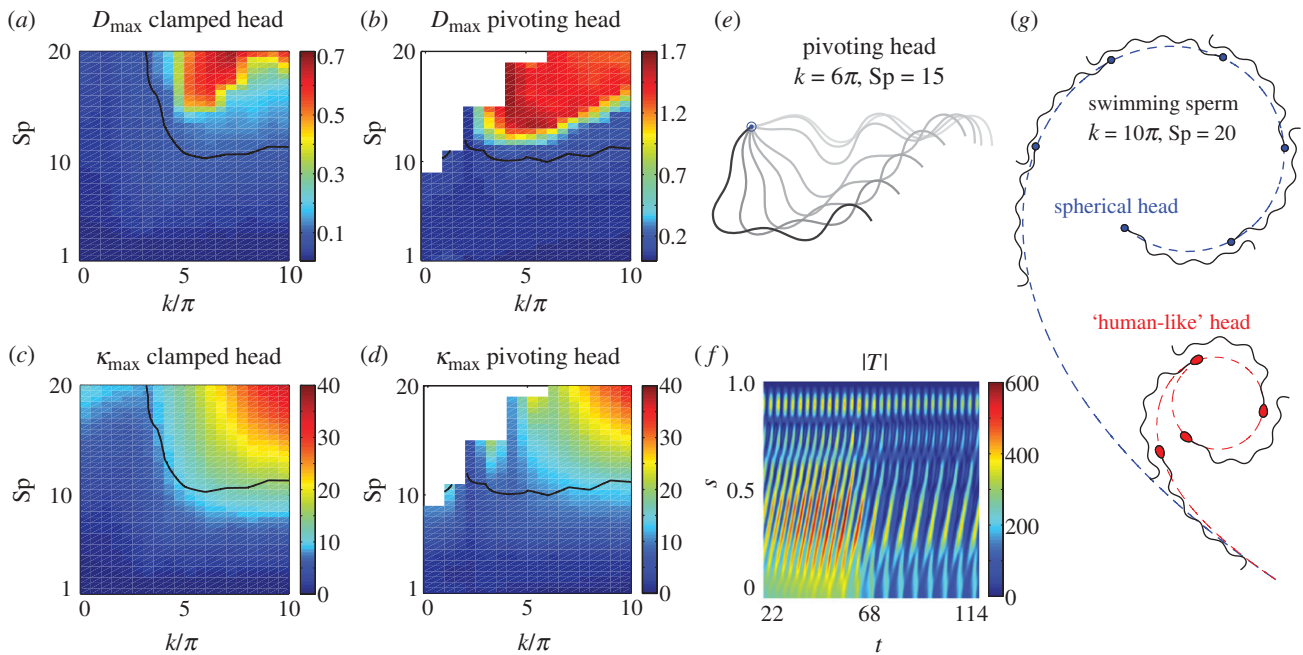


Figure 4. The breakdown of linear theory, the symmetry-breaking instability and its consequences for the free head swimmer. (a,b) The discrepancy measure,  $D_{\max} = \max_{t,s} |\mathbf{X}_N - \mathbf{X}_L|$ , is illustrated for varying internal shear wavenumber  $k$ , and sperm compliance parameter,  $Sp$ , in both the pivoting head and clamped head cases. (c,d), the maximum of the linear theory prediction of curvature,  $\kappa_{\max}$ , is presented. In all these four plots, the solid black contour marks where  $D_{\max} = 0.1$ , noting that significantly larger values are observed to characterize poor agreement between the linear and nonlinear theories. (e,f) The transient features of the symmetry-breaking bifurcation to asymmetric waveforms for the pivoting head boundary condition, when  $k = 6\pi$  and  $Sp = 15$  (figure 3g). (e) Time sequence once the flagellar buckling instability can be readily observed, with waveforms overlaid at equal time intervals with the point of attachment in blue. The initial waveform ( $t = 18.18$ ) is illustrated in light grey and the final waveform ( $t = 150.76$ ) in black, with a progression in darkness with time. (f) The associated absolute tension  $|T|$  as a function of time  $t$  and arclength  $s$ . (g) The influence of the symmetry-breaking instability on the overall trajectory and flagellar beating pattern of the free swimming cell, plotted at equal time intervals. Smoothed trajectories are plotted for two different sperm head geometries: a spherical head (dashed blue) and a ‘human-like’ head morphology (dashed red), both with the same human-like head volume (Smith *et al.* 2009a). Here, the internal shear density is given by equation (2.3) with  $k = 10\pi$  and  $Sp = 20$ , and the dimensionless force magnitude  $A$  is 75% of the force amplitude used for the pivoting case when the maximum displacement is  $0.1L$  (equation (2.4) and electronic supplementary material, figure S1). The buckling transition induces an asymmetric waveform that drives swimmers towards permanent circular paths; the swimming direction is inverted if  $f \rightarrow -f$  in equation (2.1).

path direction after buckling is sensitive to the phase of the internal shear forcing.

#### 4. DISCUSSION

Although the dynamics of an internally driven filament in viscous fluids has been widely studied, the possible influence of a nonlinear buckling instability on the ultimate flagellar patterns has not been explored. Here, we consider the physical principles of this instability in the context of flagellar dynamics, incorporating the influence of the surrounding fluid through RFT. The structural response of the flagellum is governed by geometrically nonlinear filament elasticity theory and the internal forcing is represented via the sliding filament model of eukaryotic flagellar motility. The coupling of these three physical phenomena leads to the emergence of complex flagellar waveforms, which were examined in detail through numerical simulations for a large spectrum of internal shear wavenumber,  $k$ , sperm compliance,  $Sp$ , and different boundary conditions.

While weakly nonlinear analyses (Hilfinger *et al.* 2009; Mitchison & Mitchison 2010) support the use of

geometrically linear elasticity theory in recent models of flagellar dynamics (Camalet *et al.* 1999; Camalet & Jülicher 2000; Riedel-Kruse *et al.* 2007; Fu *et al.* 2008), we have demonstrated that the linear theory can be unreliable in general. On varying the internal shear wavenumber  $k$  and the sperm compliance,  $Sp$ , the linear theory yields inaccurate predictions for reasonably large values of  $Sp$  and a wide range of wavenumbers  $k$  (figure 4a,b). While the linear model demonstrates a plausible behaviour in this parameter regime (Fu *et al.* 2008), the nonlinear simulation exposes the higher order effects and exhibits complex flagellar beating (figure 3). Physically, it is reasonable to expect an increasing inaccuracy of the linear model for larger values of  $k$  and  $Sp$ , even with constraints on flagellar waveform amplitude. In particular, higher wavenumbers continuously force the flagellum to increase its curvature locally. With higher sperm compliance parameters  $Sp$  (equation (2.2)), and thus a sufficient viscous resistance to prevent the tendency of elastic forces to reduce this curvature, high tangential forces are induced, which are nominally a second-order contribution (Camalet & Jülicher 2000; Hilfinger *et al.* 2009). Hence, the validity of the linear theory requires a larger flagellum

radius of curvature, observed to be at least 10 per cent of flagellum length, rather than constraints on the amplitude of flagellar deflection (Fu *et al.* 2008).

Our main result from this nonlinear investigation is that asymmetric flagellar waveforms may arise dynamically from intrinsically symmetric flagellar dynamics; this is not captured by linear or weakly nonlinear theories. Consequently, an asymmetric flagellar waveform can be initiated and maintained without any change in cell signalling or the presence of flagellar heterogeneity. The asymmetric flagellar bending is caused by a common phenomenon in elastic filament dynamics, the buckling instability (Becker & Shelley 2001), which is frequently found in passive filaments when subjected to high tangential forces. This mechanism is also manifested in driven flagellar dynamics (figure 3), though, conversely, it is triggered by the internal shear force via the  $\tilde{f}_n$  contribution in equation (2.1). This causes the absolute tension to rise; once beyond a critical value that the flagellum elastic structure cannot support, asymmetric bending is observed (figure 4*e,f*). Furthermore, the flagellum is still driven by the same internal shear after buckling, which continuously forces the flagellum to maintain the emerging asymmetric bending pattern: roughly an ‘S’ shape for a fixed head and a ‘C’ shape for both the pivoting head case and the swimming sperm (figures 3 and 4*g*). This represents a markedly distinct buckling instability from those reported in the literature (Bourdieu *et al.* 1995; Becker & Shelley 2001; Tornberg & Shelley 2004).

This flagellar buckling instability is readily found for large values of the internal shear wavenumber  $k$  and the sperm compliance parameter  $S_p$ ; it is also apparent for moderate wavenumbers, in particular, for constrained sperm especially when the sperm head is pivoting. While the clamped boundary condition restrains the motion, the free torque condition in the pivoting head simulations allows the sperm to rotate around its fixed point; analogously, the free head swimmer boundary conditions induce waveform asymmetries that drive circular trajectories. Furthermore, the swimming sperm trajectories are sensitive to sperm head morphology. Morphologies may subtly alter the net viscous drag on the swimming flagellum, in turn altering the tension via the boundary conditions. However, in the context of the emergent behaviour from a tension-driven buckling instability, this can have a substantial effect on the emergent waveform, and hence the resulting swimming trajectory (figure 4*g*). Furthermore, the swimming direction is a non-trivial consequence of the force and torque balance during the bifurcation to asymmetric waveforms and, in particular, exhibits a dependence on the phase of the internal sliding forces.

These results demonstrate that asymmetric flagellar beating does not necessarily require an intrinsic asymmetric forcing mechanism. Thus, observations of circular swimming or flagellar waveform asymmetry are not sufficient to infer the presence of hyperactivation or any other asymmetric physiological regulation or signalling influencing the internal dynein molecular motors within the flagellum. Similarly, one cannot immediately infer that subtle flagellar structural

asymmetries, such as the 5–6 microtubule bridging (Satir 1965; Olson & Linck 1977), are dynamically critical and driving symmetry breaking. Moreover, high wavenumbers are commonly exhibited by sperm migrating in high viscosity fluids (Smith *et al.* 2009*b*) and circling cells (figure 1). The results we have presented indicate that it is physically plausible for this behaviour to be caused by excessive tangential forces on the flagellum owing to both internal shear forces and the viscous drag on the sperm cell. Nonetheless, the influences of ultrastructural, histological and physiological complications are currently unexplored. For example, we have not considered the role of tapering in the accessory flagellar structures commonly found in mammalian sperm cells, such as the outer dense fibres. These accessory structures reinforce the flagellum in regions where high tensions are expected, and may also act to prevent the flagellar buckling instability; likewise, subtle structural asymmetries of the sperm flagellum could encourage buckling. Similarly, possible dynein detachment mechanisms at high flagellar curvature, such as the geometric clutch hypothesis (Lindemann & Kanous 1995), may influence the emergent waveform and require exploration. Further work could also account for non-local hydrodynamic effects.

In summary, our formulation is the first to explore the buckling instability of a filament driven by internal shear forces within viscous fluids. It has firstly delimited the validity of geometrically linear elastic filament theory. Secondly, the study has demonstrated the physical plausibility of dynamical symmetry breaking of filaments. Our demonstration that the asymmetric waveforms (figure 1 and electronic supplementary material, movie S1) that characterize specialized sperm behaviours, such as hyperactivation or chemotaxis, can also emerge dynamically without recourse to variations in structure or signalling (figures 3 and 4*g*), emphasizes the importance of being alert to this symmetry-breaking mechanism when interpreting observations of sperm flagella. These findings are crucial when considering motility at these scales in physiological fluids and their analogues, because of the fact that increased viscosity induces a higher sperm compliance number, as defined in equation (2.2). Furthermore, mathematical models exploring the oscillatory behaviour of cilia and flagella beating should also consider geometrically nonlinear dynamics to accommodate the high curvatures observed physiologically. We hope these findings will stimulate future mathematical research, which considers the role for geometrically nonlinear dynamics and buckling instabilities in other systems exhibiting flagellar motility, such as protozoa, algae and artificial microswimmers.

The authors thank Mr Henry Shum for many helpful discussions and Professor John R. Blake for continued insight. H.G. acknowledges the Capes Foundation (Brazilian sponsor) for financial support through grant no. BEX 4676/06-8, and also through the Hester Cordelia Parsons Fund and Timothy Bailey Trust. D.J.S. thanks the Medical Research Council through grant no. G0600178. This publication is based on work supported in part by Award no. KUK-C1-013-04, made by King Abdullah University of Science and Technology (KAUST).



## REFERENCES

- Baltz, J. M., Williams, P. O. & Cone, R. A. 1990 Dense fibers protect mammalian sperm against damage. *Biol. Reprod.* **43**, 485–491. (doi:10.1095/biolreprod43.3.485)
- Becker, L. E. & Shelley, M. J. 2001 Instability of elastic filaments in shear flow yields first-normal-stress differences. *Phys. Rev. Lett.* **87**, 198 301–198 304. (doi:10.1103/PhysRevLett.87.198301)
- Bourdieu, L., Duke, T., Elowitz, M. B., Winkelmann, D. A., Leibler, S. & Libchaber, A. 1995 Spiral defects in motility assays: a measure of motor protein force. *Phys. Rev. Lett.* **75**, 176–179. (doi:10.1103/PhysRevLett.75.176)
- Brokaw, C. J. 1971 Bend propagation by a sliding filament model for flagella. *J. Exp. Biol.* **55**, 289–304.
- Brokaw, C. J. 1975 Molecular mechanism for oscillation in flagella and muscle. *Proc. Natl Acad. Sci. USA* **72**, 3102–3106. (doi:10.1073/pnas.72.8.3102)
- Brokaw, C. J. 2009 Thinking about flagellar oscillations. *Cell Motil. Cytoskeleton* **66**, 425–436. (doi:10.1002/cm.20313)
- Camalet, S. & J ulicher, F. 2000 Generic aspects of axonemal beating. *New J. Phys.* **2**, 24.1–24.23.
- Camalet, S., J ulicher, F. & Prost, J. 1999 Self-organized beating and swimming of internally driven filaments. *Phys. Rev. Lett.* **82**, 1590–1593. (doi:10.1103/PhysRevLett.82.1590)
- Fawcett, D. W. 1975 The mammalian spermatozoon. *Dev. Biol.* **44**, 394–436.
- Fu, H. C., Wolgemuth, C. W. & Powers, T. R. 2008 Beating patterns of filaments in viscoelastic fluids. *Phys. Rev. E* **78**, 041 913–041 925. (doi:10.1103/PhysRevE.78.041913)
- Goldstein, R. E. & Langer, S. A. 1995 Nonlinear dynamics of stiff polymers. *Phys. Rev. Lett.* **75**, 1094–1097. (doi:10.1103/PhysRevLett.75.1094)
- Goldstein, R. E., Powers, T. R. & Wiggins, C. H. 1998 Viscous nonlinear dynamics of twist and writhe. *Phys. Rev. Lett.* **80**, 5232–5235. (doi:10.1103/PhysRevLett.80.5232)
- Goldstein, S. F. 1977 Asymmetric waveforms in echinoderm sperm flagella. *J. Exp. Biol.* **71**, 157–170.
- Gray, J. & Hancock, G. J. 1955 The propulsion of sea-urchin spermatozoa. *J. Exp. Biol.* **32**, 802–814.
- Gueron, S. & Liron, N. 1993 Simulations of three-dimensional ciliary beats and cilia interactions. *Biophys. J.* **65**, 499–507. (doi:10.1016/S0006-3495(93)81062-2)
- Hilfinger, A. & J ulicher, F. 2008 The chirality of ciliary beats. *Phys. Biol.* **5**, 016 003–016 015. (doi:10.1088/1478-3975/5/1/016003)
- Hilfinger, A., Chattopadhyay, A. K. & J ulicher, F. 2009 Nonlinear dynamics of cilia and flagella. *Phys. Rev. E* **79**, 051 918–051 925. (doi:10.1103/PhysRevE.79.051918)
- Hines, M. & Blum, J. 1978 Bend propagation in flagella. I. Derivation of equations of motion and their simulation. *Biophys. J.* **23**, 41–57. (doi:10.1016/S0006-3495(78)85431-9)
- Johnson, R. E. 1980 An improved slender-body theory for stokes flow. *J. Fluid Mech.* **99**, 411–431. (doi:10.1017/S0022112080000687)
- Johnson, R. E. & Brokaw, C. J. 1979 Flagellar hydrodynamics. A comparison between resistive-force theory and slender-body theory. *Biophys. J.* **25**, 113–127. ISSN 0006-3495. (doi:10.1016/S0006-3495(79)85281-9)
- Katz, D. F., Drobnis, E. & Overstreet, J. W. 1989 Factors regulating mammalian sperm migration through the female reproductive tract and oocyte vestments. *Gamete Res.* **22**, 443–469. (doi:10.1002/mrd.1120220410)
- Kinukawa, M., Nagata, M. & Aoki, F. 2003 Changes in flagellar bending during the course of hyperactivation in hamster spermatozoa. *Reproduction* **125**, 43–51. (doi:10.1530/rep.0.1250043)
- Lindemann, C. & Kanous, K. 1995 ‘Geometric clutch’ hypothesis of axonemal function: key issues and testable predictions. *Cell. Motil. Cytoskeleton* **31**, 1–8. (doi:10.1002/cm.970310102)
- Lindemann, C. B., Orlando, A. & Kanous, K. S. 1992 The flagellar beat of rat sperm is organized by the interaction of two functionally distinct populations of dynein bridges with a stable central axonemal partition. *J. Cell Sci.* **102**, 249–260.
- Lindemann, C. B., Macauley, J. A. & Lesich, K. A. 2005 The counterbend phenomenon in dynein-disabled rat sperm flagella and what it reveals about the interdoublet elasticity. *Biophys. J.* **89**, 1165–1174. (doi:10.1529/biophysj.105.060681)
- Machin, K. E. 1958 Wave propagation along flagella. *J. Exp. Biol.* **35**, 796–806.
- Miller, R. L. & Brokaw, C. J. 1970 Chemotactic turning behaviour of tubularia spermatozoa. *J. Exp. Biol.* **52**, 699–706.
- Mitchison, T. J. & Mitchison, H. M. 2010 Cell biology: how cilia beat. *Nature* **463**, 308–309. (doi:10.1038/463308a)
- Olson, G. E. & Linck, R. W. 1977 Observations of the structural components of flagellar axonemes and central pair microtubules from rat sperm. *J. Ultrastruct. Res.* **61**, 21–43. (doi:10.1016/S0022-5320(77)90004-1)
- Riedel-Kruse, I. H., Hilfinger, A., Howard, J. & J ulicher, F. 2007 How molecular motors shape the flagellar beat. *HFSP* **1**, 192–208. (doi:10.2976/1.2773861)
- Satir, P. 1965 Studies on cilia: II. Examination of the distal region of the ciliary shaft and the role of the filaments in motility. *J. Cell Biol.* **26**, 805–834. (doi:10.1083/jcb.26.3.805)
- Smith, D. J., Gaffney, E. A., Blake, J. R. & Kirkman-Brown, J. C. 2009a Human sperm accumulation near surfaces: a simulation study. *J. Fluid Mech.* **621**, 289–320. (doi:10.1017/S0022112008004953)
- Smith, D. J., Gaffney, E. A., Gad elha, H., Kapur, N. & Kirkman-Brown, J. C. 2009b Bend propagation in the flagella of migrating human sperm, and its modulation by viscosity. *Cell Motil. Cytoskeleton* **66**, 220–236. (doi:10.1002/cm.20345)
- Suarez, S. S. & Ho, H. C. 2003 Hyperactivated motility in sperm. *Reprod. Domest. Anim.* **38**, 119–124. (doi:10.1046/j.1439-0531.2003.00397.x)
- Tornberg, A. K. & Shelley, M. J. 2004 Simulating the dynamics and interactions of flexible fibers in stokes flows. *J. Comput. Phys.* **196**, 8–40. (doi:10.1016/j.jcp.2003.10.017)
- Ward, G. E., Brokaw, C. J., Garbers, D. L. & Vacquier, V. D. 1985 Chemotaxis of *Arbacia punctulata* spermatozoa to resact, a peptide from the egg jelly layer. *J. Cell Biol.* **101**, 2324–2329. (doi:10.1083/jcb.101.6.2324)
- Wiggins, C. H., Rivelino, D., Ott, A. & Goldstein, R. E. 1998 Trapping and wiggling: elastohydrodynamics of driven microfilaments. *Biophys. J.* **74**, 1043–1060. (doi:10.1016/S0006-3495(98)74029-9)
- Wolgemuth, C. W., Powers, T. R. & Goldstein, R. E. 2000 Twirling and whirling: viscous dynamics of rotating elastic filaments. *Phys. Rev. Lett.* **84**, 1623–1626. (doi:10.1103/PhysRevLett.84.1623)
- Woolley, D. M. 2003 Motility of spermatozoa at surfaces. *Reproduction* **126**, 259–270. (doi:10.1530/rep.0.1260259)
- Yu, T. S., Lauga, E. & Hosoi, A. E. 2006 Experimental investigations of elastic tail propulsion at low reynolds number. *Phys. Fluids* **18**, 0 917 011–0 917 014. (doi:10.1063/1.2349585)